Benefits of Silica Core-Shell Structures on the Temperature Sensing Properties of Er,Yb:$GdVO_4$ Up-Conversion Nanoparticles

Oleksandr A. Savchuk,[1] Joan J. Carvajal,[1] C. Cascales,[2] M. Aguiló,[1] F. Díaz[1]*

[1]Physics and Crystallography of Materials and Nanomaterials (FiCMA-FiCNA) and EMaS, Universitat Rovira i Virgili (URV), Marcel·lí Domingo 1, Tarragona, 43007, Spain

[2]Instituto de Ciencia de Materiales de Madrid, c/ Sor Juana Inés de la Cruz, Cantoblanco, Madrid, 28049, Spain

Corresponding Author

*joanjosep.carvajal@urv.cat

Abstract

We studied the temperature dependent luminescence of $GdVO_4$ nanoparticles co-doped with Er^{3+} (1 mol%) and Yb^{3+} (20 mol%) and determined their thermal sensing properties through the fluorescence intensity ratio (FIR) technique. We also analyzed how a silica coating, in a core-shell structure, affects the temperature sensing properties of this material. Spectra were recorded in the range of biological temperatures (298–343 K). The absolute sensitivity for temperature determination calculated for the core-shell nanoparticles is double than the one calculated for bare nanoparticles, achieving a thermal resolution of 0.4 K. Moreover, silica-coated nanoparticles show good dispersibility in different solvents, such as water, DMSO and methanol. Also, they show good luminescence stability without interactions with solvent molecules. Furthermore, we also observed that the silica coating shell prevents from a progressive heating of the nanoparticles during prolonged excitations periods with the 980 nm laser, preventing effects on their thermometric applications.

TOC GRAPHICS

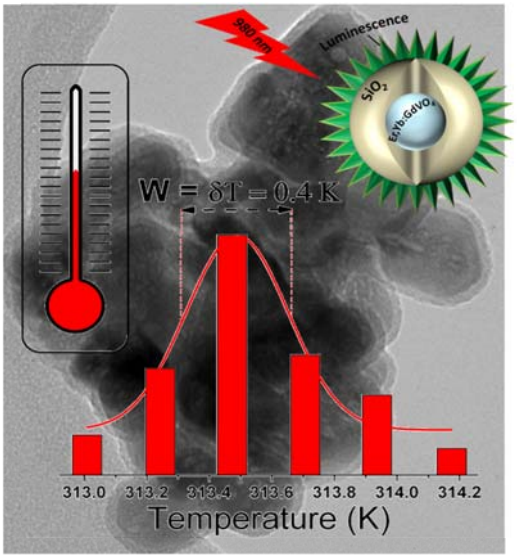

KEYWORDS: luminescence, thermometry, core-shell, up-conversion, nanosensors.

1. Introduction

Temperature is the most frequently measured physical property in science, industries and life. Many properties of matter depend on temperature, thus, it is important to monitor it during material processing for controlling the quality of the final products as well as in biomedical areas, where temperature provides basic diagnostic criteria.[1,2]

To overcome the problems evidenced in conventional contact thermometry methods (invasiveness and big sizes), non-contact thermometry methods have been developed.[3,4] Among these methods, luminescence nanothermometry, and particularly luminescence nanothermometry based on measurements of the fluorescence intensity ratio (FIR) is particularly interesting, since it can prevent errors in measurements arising from power fluctuations of the excitation source,

variations on the concentration of luminescent nanoparticles and inhomogenities of the material.[5] The FIR method is based in the Boltzmann distribution of electrons between two adjacent emitting energy levels, that depends on temperature, and is manifested as a temperature-dependent intensity ratio between the emissions arising from two distinct lines in the spectrum. Furthermore, the FIR technique constitutes a self-referencing method to compute the absolute temperature, since one spectrum contains all the information needed, avoiding the use of an internal reference.[3]

Trivalent lanthanide (Ln)-doped nanoparticles (NPs) are among the most promising candidates for temperature determination through luminescence thermometry. Optically active Ln cations show several narrow absorption and emission lines, some of them from excited states lying very close in energy that can be considered to be thermally coupled. They also show relatively long emission lifetimes, and good chemical and physical stability.[6-8]

Most of the work developed up to now on ratiometric luminescence nanothermometry by the FIR technique was performed using Er^{3+} doped[9-11] and Er^{3+}/Yb^{3+} co-doped materials.[6,11-18] Er^{3+} shows an efficient green up-conversion emission from two thermally coupled excited states, $^2H_{11/2}$ and $^4S_{3/2}$, upon NIR excitation at 980 nm. Yb^{3+} is used as a sensitizer since it shows a higher absorption cross-section at this wavelength. Furthermore, the energy transfer between Yb^{3+} and Er^{3+} is very efficient. This allows generating a bright emission in the visible, especially in the green. Er^{3+}/Yb^{3+} co-doped NPs have been used, for instance, to show the temperature evolution of cancer HeLa cells up to its thermally induced death[7] or to determine the temperature in human embryo kidney cells.[19]

Despite the significant progress achieved in recent years on luminescence thermometry using Ln-doped NPs, there are still several aspects that need to be improved, such as sensitivity to

determine smaller temperature changes. For instance, it was demonstrated that the combination of Ln-doped NPs with a thermosensitive polymer can enhance this thermal sensitivity.[20] Also, the sensitivity and the temperature sensing range can be tuned in organic-inorganic complexes based on Ln ions just by changing the chelate ligands on the Ln-complexes or the host in which the luminescent centers were embedded.[21]

The benefits of core-shell structures to enhance the emission properties of up-conversion nanoparticles has already been reported.[22] Here, we report the enhancement of the luminescence temperature sensitivity in Er,Yb:$GdVO_4$ nanoparticles coated with a silica shell that allowed to get a thermal resolution of 0.4 K. Furthermore, we probed that the as-synthesized Er,Yb:$GdVO_4$@SiO_2 core-shell nanoparticles are dispersible in biological compatible fluids that facilitate their potential biological applications. Finally, we also observed that the silica shell prevents the heating of the luminescent nanoparticles when excited for prolonged periods at 980 nm.

2. Experimental Section

2.1 Synthesis of luminescent nanoparticles.

Crystalline NPs of $GdVO_4$ codoped with Er^{3+} (1 mol%) and Yb^{3+} (20 mol%) were prepared by a hydrothermal process. Details of the synthesis can be found elsewere.[23] Shortly, NH_4VO_3 and lanthanide nitrates ($Gd(NO_3)_3{\cdot}6H_2O$, $Yb(NO_3)_3{\cdot}6H_2O$, $Er(NO_3)_3{\cdot}6H_2O$ (Strem Chemicals 99.99%) were used as reactants. The first step involved the preparation of a solution with the required amounts of lanthanide nitrates and NH_4VO_3 in distilled water (40 ml), in which the pH was adjusted to 7 by adding diluted NH_4OH under stirring during 1 h. The yellow dispersion was

afterwards hydrothermally treated at 458 K during 24 h in a sealed Teflon-lined autoclave with a capacity of 75 ml. The product obtained was separated by centrifugation, washed several times with distilled water and overnight dried at 393 K in open air.

To improve their emission efficiency, the samples were then annealed to 873 K for 5 h. Further coating of the NPs surface with a layer of silica (SiO_2) (Er,Yb:$GdVO_4$@SiO_2) was carried out through the base-catalyzed hydrolysis of tetraetoxysilane ($Si(OC_2H_5)_4$, TEOS, Alfa Aesar 99%) and the subsequent condensation of silanol (Si-OH) groups onto the surface of the Er,Yb:$GdVO_4$ NPs. To do that, a half of the prepared amount of NPs was dispersed in an ethanolic solution (40 ml ethanol absolute 99.5% Emplura Merck + 4 ml distilled water) in which the pH was adjusted to 9 with diluted NH_4OH, and then 2 ml of TEOS were added and kept under stirring for 4 h. The product was finally washed with ethanol, centrifuged and dried to 393 K.

2.2 Structural characterization and particle size determination.

1 mol% Er, 20 mol% Yb:$GdVO_4$ and 1 mol% Er, 20 mol% Yb:$GdVO_4$@SiO_2 NPs were characterized by powder X-ray diffraction (XRD) using a Bruker AXS D-8 Advance diffractometer with Cu Kα radiation. Transmission electron microscopy (TEM) images were obtained with a JEOL 2000FXII microscope with an accelerating voltage of 200 kV. High resolution TEM (HRTEM) and selected area electron diffraction (SAED) images were obtained with a JEOL model JEM-4000EX microscope, with an accelerating voltage of 400 kV. Hydrodynamic particle size distributions were measured by dynamic light scattering (DLS) using a Vasco 2-Cordouan equipment, with samples dispersed in distilled water. Fourier transform

infrared absorption (FT-IR) data were collected on a Nicolet 20SXC spectrophotometer in the range 4000 – 400 cm^{-1}, using KBr to prepare pellets of the analyzed materials.

2.3 Spectroscopic characterization

For the analysis of the temperature dependent up-conversion emission, Er,Yb:$GdVO_4$ and Er,Yb:$GdVO_4$@SiO_2 NPs were introduced in a heating stage Linkam THMS 600 that was placed in a homemade microscope setup. An Apollo Instruments Inc diode laser with emission at 980 nm and a power of 100 mW was used as the excitation source. The laser beam was focused on the sample using a microscope objective with 40X magnification and N.A. of 0.6 that produced a laser spot of around 10 μm on the sample. The emission was collected by the same microscope objective, and after passing a dichroic filter to eliminate the excitation radiation, was collected by an AVANTES AVS-USB2000 fiberoptic spectrometer connected to a computer to record the spectra.

Spectra were also collected using a Labsphere 4GPS-020-SL integrating sphere to compare the intensity of the spectra generated by the different samples, using the same fiberoptic spectrometer described above to record the spectra.

3. Results and Discussion

3.1 Structural characterization

The XRD pattern of the raw 1% Er, 20% Yb:$GdVO_4$ nanoparticles corresponds to the pure tetragonal $I4_1/amd$ zircon-type phase (see Figure 1). By using the Scherrer's equation, the mean individual crystalline domains (also called 'crystallites') calculated from the full width at half maximum (FWHM) of the Bragg peak located at ~25 º 2θ is ~25 nm, see Figure 1(b). No additional reflections were detected for 1% Er, 20% Yb:$GdVO_4$@SiO_2 core-shell nanoparticles, see Figure 1(c), although the somewhat rougher background reflects the presence of amorphous SiO_2. The XRD pattern of NPs coated with thicker silica shells (not included in the current study) revealed that the roughness of the background at 18-32º 2θ was, as expected, considerably accentuated, see Figures S1(a-c) included in the Supplementary Information.

Figures 1(d) and 1(f) display typical TEM images of Er,Yb:$GdVO_4$ and Er,Yb:$GdVO_4$@SiO_2 NPs, respectively, mainly with square and rounded sections, and Figures 1(e) and 1(g) display HRTEM images of these samples. Darker interiors and surrounding lighter shells in the TEM and HRTEM images of NPs in Figures 1 (f) and 1(g) correspond to Er,Yb:$GdVO_4$ cores and their amorphous silica coating, respectively. It is observed that the coating layer has a thickness of ~7 nm around the NPs, which mostly retain their initial polygonal or rounded shape. A characteristic TEM image of a sample in which the vanadate NPs were coated with a thicker silica shell can be seen in the Supplementary Information, Figure S2. HRTEM images of discrete NPs reveal in all cases a well-defined single crystal structure, characteristic of the tetragonal $I4_1/amd$ symmetry of $GdVO_4$ (see further images in Figures S3a-d). From the lattice fringes in Figure S3(a), as well as

the corresponding selected area electron diffraction (SAED) pattern in Figure S3(b), the resolved interplanar spacings are found to be about 0.359 nm, consistent with the *d*-spacing between (200) planes of $GdVO_4$ (JCPDS File 86-0996).

FT-IR spectra for the raw hydrothermal, 873 K annealed, and annealed and further silica coated 1%Er, 20% Yb:$GdVO_4$ samples, whose XRD patters are shown in Figures 1(a-c), are provided in Figures S4(a-c) of the Supplementary Information, along with the discussion for vibronic assignments accounting for the formation of the Ln:GdVO4@SiO_2 entity, which further probe the silica shell formation on the nanoparticles.

Figures S5(a),(b) included in the Supplementary Information show characteristic results from DLS measurements on the particle size (hydrodynamic size) distribution for both 873 K annealed and ~ 7nm silica-coated Er, Yb:$GdVO_4$ samples.

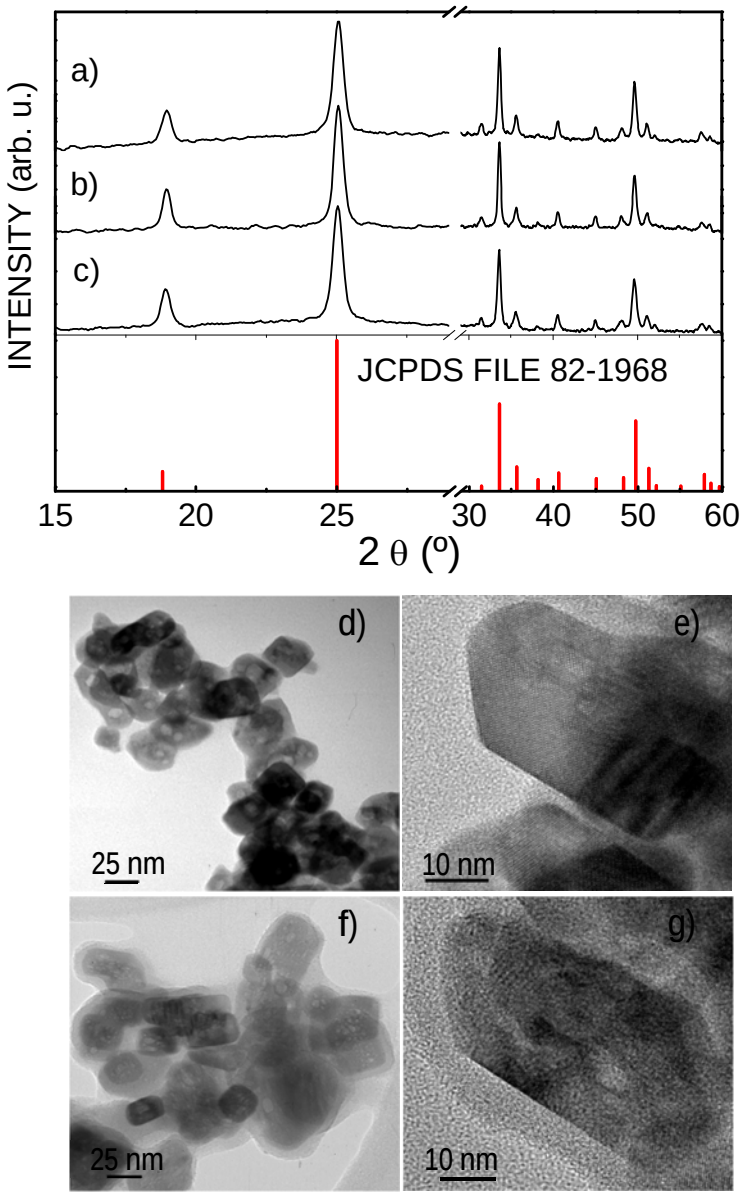

Figure 1. X ray diffraction patterns of (a) raw hydrothermal 1 % Er, 20 %Yb:$GdVO_4$, (b) 1 % Er, 20 %Yb:$GdVO_4$ after 873 K thermal annealing during 5 h, and (c) the annealed sample in (b) with further SiO_2 coating, 1 % Er, 20 %Yb:$GdVO_4$@SiO_2. For comparison, the XRD pattern scheme of tetragonal $I4_1/amd$ YVO_4, JCPDS File 82-1968 has been also included. TEM images of (d) Er,Yb:$GdVO_4$ and (f) Er,Yb:$GdVO_4$@SiO_2 nanoparticles. HRTEM images of (e) Er, Yb:$GdVO_4$ and (g) Er, Yb:$GdVO_4$@SiO_2 nanoparticles.

3.2 Spectroscopic characterization

Nanoparticles were placed in a borosilicate bottom flat vial and compacted to ensure that they fill the bottom of the vial. This vial was introduced in a sample holder that was placed inside a Labsphere 4GPS-020-SL integrating sphere. Then, the samples were excited with a 200 μm core diameter fiber-coupled laser diode from Apollo Instruments, Inc. emitting at 980 nm. The laser was collimated to a spot size of 3 mm on the sample, and a power of 100 mW. The emission arising from the NPs was collected using an AVANTES AVS-USB2000 fiberoptic spectrometer. The inner part of the integrating sphere is made from a diffusive material that facilitates the luminescence generated by the NPs to spread evenly by multiple reflections over the entire sphere surface before being collected by the detectors. In this way, all the light emitted by the sample is collected by the detector, allowing us to compare the intensity of the emission generated by the different samples.

Figure 2 shows the up-conversion photoluminescence emission spectra of Er,Yb:$GdVO_4$ and Er,Yb:$GdVO_4$@SiO_2 core-shell NPs after excitation at NIR 980 nm collected in the integrating sphere. The up-conversion emission spectra of these samples consist on two main bands centered at 520 and 550 nm, which correspond to the $^2H_{11/2} \rightarrow {}^4I_{15/2}$ and $^4S_{3/2} \rightarrow {}^4I_{15/2}$ transitions of the Er^{3+} ion, respectively. Also a weak red band was observed at 640-670 nm, assigned to the $^4F_{9/2} \rightarrow {}^4I_{15/2}$ transition of Er^{3+}. Splittings of all optical transitions in the Figure 2 are similar to those reported for Er-doped single crystal, indicating that the crystal site for Er^{3+} is kept in the prepared nanoparticles.[23] In Figure 2, however, the emission bands presented are broad, due to the conditions of detection we had to use because of the low intensity of the emissions in the integrating sphere. Since the concentration of doping ions in both cases was identical, Figure 2

represents the comparison of the corresponding fluorescence efficiencies. It can be seen that the emission intensity is higher for Er,Yb:$GdVO_4$@SiO_2 core-shell NPs. This enhancement might be due to the reduction of surface defects on the core-shell NPs due to the presence of the inert SiO_2 coating.[24]

To further confirm this enhancement of the emission intensity generated by the silica coating, Figures S6(a),(b) in the Supporting Information display the evolution of the integrated intensity of the visible upconverted emissions for Ln, Yb:$GdVO_4$ NPs as a function of the surface treatment (annealing and silica coating) after the hydrothermal synthesis. As can be seen in the figure, 1% Er, 20%Yb:$GdVO_4$ NPs coated with a ~7 nm silica shell show the highest upconversion efficiency.

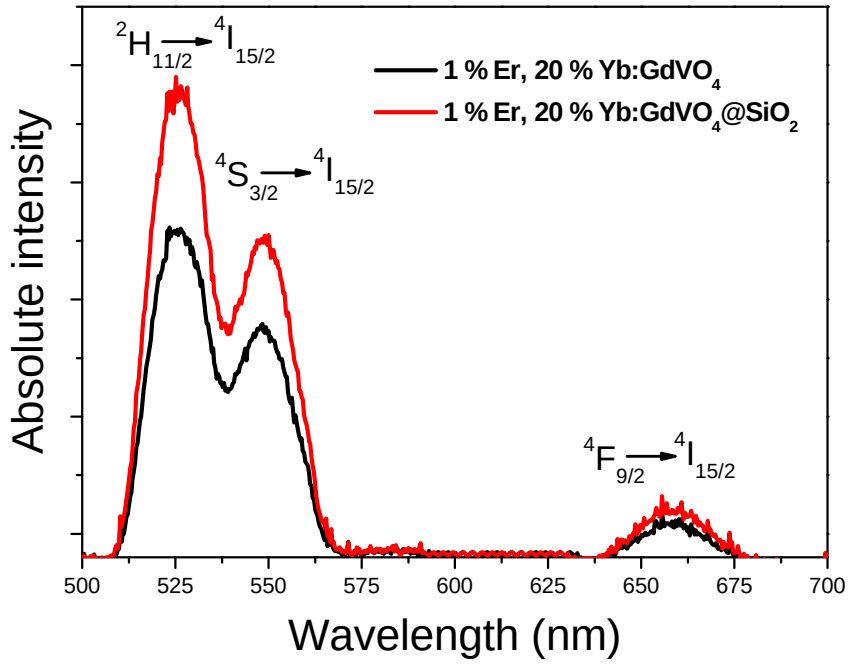

Figure 2. Up-conversion emission spectra of the 1%Er, 20%Yb:$GdVO_4$ nanoparticles and 1%Er, 20%Yb:$GdVO_4$@SiO_2 core-shell nanoparticles after excitation at 980 nm.

3.3 Luminescence thermometry

In order to find out the effect of the silica coating on the temperature sensing capabilities of our NPs, we measured the dependence of the up-conversion emission spectra with temperature for both samples in the biological range. This thermal characterization was made using the FIR technique, using the following equation:[5]

$$FIR = \frac{I_1}{I_2} = \frac{g_1 v_1 \sigma_1}{g_2 v_2 \sigma_2} = B \exp\left(-\frac{\Delta E}{k_B T}\right) \quad (1)$$

where g_i, v_i, and σ_i, are the level degeneracy, the spontaneous emission, and the absorption rates, respectively, k_B is the Boltzmann constant, T is the absolute temperature, and ΔE is the energy difference between the two energy states considered.

Figure 3(a) shows the changes in the normalized intensity of the spectra in the green region recorded for the Er,Yb:$GdVO_4$@SiO_2 core-shell NPs at room temperature and at the maximum temperature analyzed in this work (343 K). As can be seen, while the intensity of the emission arising from the $^2H_{11/2}$ level increases substantially when the temperature increased. Figure 3(b) shows the evolution of the FIR with temperature of both kinds of NPs. In the two cases they follow a linear tendency with regression coefficients of 0.992 and 0.987 for Er,Yb:$GdVO_4$ and Er,Yb:$GdVO_4$@SiO_2 core-shell NPs, respectively. The slope is higher for core-shell NPs. This results in a higher absolute sensitivity, calculated as the first derivative of the FIR to respect temperature, as shown in Figure 3(c). The maximum absolute sensitivity of Er,Yb:$GdVO_4$@SiO_2 core-shell NPs was found to be 1.01 % K^{-1}, almost double than the one obtained for the bare nanoparticles (0.69 % K^{-1}). In order to compare the sensitivity of the Er,Yb:$GdVO_4$@SiO_2 core-shell NPs with other Er-doped materials for which the FIR technique was applied to determine

temperature using the same electronic transitions we used in this work, we calculated the relative sensitivity, as the first derivative of the FIR to respect temperature divided by the FIR. The comparison is presented in Table 1.

Table 1. Comparison of Er-doped materials used for luminescence nanothermometry using the FIR technique in the green region of the electromagnetic spectrum.

Material	*Temperature range (K)*	*Excitation wavelength (nm)*	*Wavelength ratio*	*Relative sensitivity %K^{-1} (temperature, K)*	*Thermal resolution (K)*	*Ref.*
Er,Yb:CaF_2	298-323	920	538/522	2.3	-	25
Er,Yb:Gd_2O_3/Au NPs	300-1050	980	510-565	1.51	1	12
Er,Yb:PbF_2	290-325	975	523/548	1.1(310)	-	13
Er,Yb:Fluoride glass	335-375	975	523/548	1.1(342)	0.8	14
Er/Er,Yb:Chalcogenide glass	293-498	1540/1060	530/555	1.05/0.52	0.3/0.5	11
Er,Yb:$NaYF_4$	299-336	920	525/545	1.0	-	6
Er,Yb:$GdVO_4$@SiO_2	297-343	980	520/550	0.94 (343)	0.4	this work
Er:ZnO	273-573	978	536/553	0.62 (443)	-	9
Er:$BaTiO_3$	322-466	980	547/526	0.52(333)	-	10
Er,Yb:Al_2O_3	295-973	978	534/549	0.52(476)	0.3	15
Er,Mo:$Yb_3Al_5O_{12}$	395-973	976	522/546	0.48(467)	0.3	25
Er,Yb:Fluoride glass	296-448	1480	522/543	0.4	1	16
Er,Yb:Gd_2O_3	300-900	980	523/548	0.39(300)		17
Er,Yb:silica glass	296-723	978	526/549	0.33(296)	0.2	18

In comparison with other Er-doped materials our results lye in the upper relative sensitive range, with values around 1 % K^{-1} or higher. Er,Yb:CaF_2[25] and Er,Yb:Gd_2O_3/Au[12] NPs show higher relative sensitivities, with values of 2.3 and 1.51 % K^{-1}, respectively, while Er,Yb:PbF_2,[13] Er,Yb:fluoride[14] and Er:chalcogenide[11] glasses, and Er,Yb:$NaYF_4$[6] nanoparticles show similar values than Er,Yb:$GdVO_4$@SiO_2 core-shell nanoparticles. In the case of Er,Yb:PbF_2, despite its high sensitivity, its spatial resolution is limited by the size of the NPs (<500 nm). Thus, the main application proposed for this material is the thermal characterizations of devices.[13] For the rest of

the materials listed in the table, the reported relative sensitivities are lower than that of Er,Yb:$GdVO_4$@SiO_2 core-shell NPs. In terms of thermal resolution, the 0.4 K that can be achieved with our NPs are only surpassed by the values reported for Er,Yb:silica glass[18], Er,Mo:$Yb_3Al_5O_{12}$,[26] Er,Yb:Al_2O_3[15] and Er/Er,Yb:chalcogenide glass.[11] However, in all these cases the thermal resolution was estimated from the sensitivity values, and not measured experimentally. Thus, our results are the first ones to confirm the thermal resolution that can be achieved with Er^{3+}-based up-conversion nanoparticles.

Apart from the data included in the table, it is also worthy to note that Sedlmeier et al. analyzed the luminescent thermometric properties of Er,Yb:$NaYF_4$@$NaYF_4$ core-shell nanoparticles, capped with citric acid (CA), and compared them with those of bare Er,Yb:$NaYF_4$ nanoparticles capped with ethylene diamine tetraacetic acid (EDTA) and CA.[27] The slope of the FIR ratio in the three cases was similar, being a little smaller for Er,Yb:$NaYF_4$ NPs capped with CA, but no difference was found between Er,Yb:$NaYF_4$@$NaYF_4$ core-shell CA-capped NPs and Er,Yb:$NaYF_4$ EDTA-capped NPs. Only the thermal resolution was improved by 5 times when the $NaYF_4$ shell was used, although again, the thermal resolution was estimated form the FIR adjusted curves.

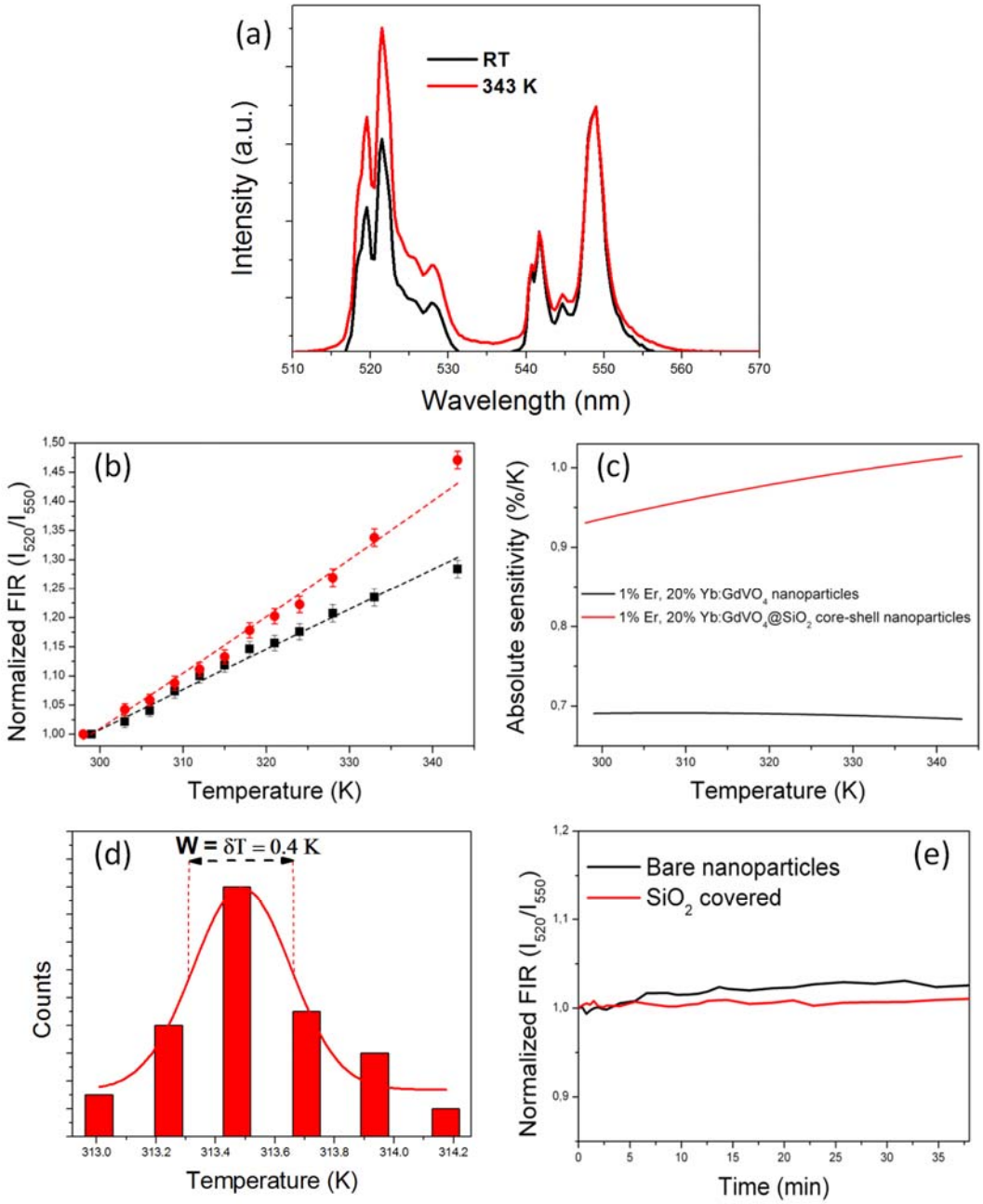

Figure 3. (a) Evolution of the intensity of the emission spectra of Er^{3+} in the green region obtained from Er,Yb:$GdVO_4$@SiO_2 NPs; (b) $I[^2H_{11/2}]/I[^4S_{3/2}]$ FIR as the function of temperature for Er,Yb:$GdVO_4$ and Er,Yb:$GdVO_4$@SiO_2 NPs; (c) Comparison of absolute sensitivity values for both kind of NPs; (d) Thermal resolution measured for Er,Yb:$GdVO_4$@SiO_2 NPs; (e) Time evolution of the intensity ratio for Er,Yb:$GdVO_4$ and Er,Yb:$GdVO_4$@SiO_2 NPs.

To know the minimum temperature change that Er,Yb:$GdVO_4$@SiO_2 NPs can discriminate, we collected 60 consecutive emission spectra at a fixed temperature (313 K) in the Linkam 600 heating stage, controlled with its embedded thermocouple. In this way we were able to determine the range of variability in the measurements.[28] Then, we calculated the temperature corresponding to each spectra using the calibration curve shown in Figure 3(b). This results in a Gaussian distribution of temperatures centered at 313.5 K with a FWHM of 0.4 K, as can be seen in Figure 3(d). This gives an estimation of the thermal resolution that can be achieved in a measurement with these NPs.

We also analysed the effect of the illumination during a prolonged time with the 980 nm laser. For this, we introduced the NPs in the Linkam 6000 heating stage, although we kept the nanoparticles at room temperature, and recorded the luminescent spectra at intervals of 10 s during 40 min. By calculating the FIR for each spectra and comparing it with the calibration curve displayed in Figure 3(b), we could plot the temporal evolution of the FIR, as can be seen in Figure 3(e). It can be seen in this graph that the FIR corresponding to the core-shell NPs remains constant under the pumping laser at 980 nm over an extended illumination period, while for the bare NPs the FIR increases, slightly but continuously, with time. This would indicate that the population of the $^2H_{11/2}$ electronic level would increase when the exposure to the excitation laser is prolonged, and thus that the Er,Yb:$GdVO_4$ NPs increase their own temperature, introducing an incorrect temperature determination. In the graph it can also be observed that these effects are evident after 7 min of continuous excitation. We repeated this experiment several times to confirm this effect, observing always similar results. Also, since the NPs were located in the heating stage during the experiment, we could also use the screen of the controller of this device

to monitor the temperature evolution, measured in that case by the internal thermocouple of the heating stage, observing the same tendency. So, an additional benefit of the silica shell with which we coated our Er,Yb:$GdVO_4$ nanoparticles is that it dissipates more effectively the heat generated in the body of NPs by the excitation laser, avoiding their heating, and providing a more stable thermal probe.

3.4 Dispersibility in different solvents

An additional advantage of the SiO_2 coating in our nanoparticles is that it allows stablishing H bridge bonds with protic polar solvents, like H_2O or methanol (CH_3OH), or van der Walls weak interactions with aprotic polar solvents, like dimethyl sulfoxide (DMSO, CH_3SOCH_3). This would allow the dispersion of the Er,Yb:$GdVO_4$@SiO_2 core-shell NPs in these kinds of solvents. We tested the possibility of dispersing our core-shell nanoparticles in these three solvents. For that, 10 mg of Er,Yb:$GdVO_4$@SiO_2 nanoparticles were dispersed in 10 ml of H_2O, methanol and DMSO, respectively, with the aid of an ultrasonic bath, and observed their sedimentation as a function of time. The results are shown in Figure 4(a). In general, the nanoparticles show a good stability in the three solvents analyzed, although after 24 h, it was reduced significantly in DMSO. These results indicate that Er,Yb:$GdVO_4$@SiO_2 NPs might be dispersed, if required in biological compatible fluids for temperature determination in biomedical applications.

We also analyzed how the different solvents affected to the up-conversion emission properties of Er,Yb:$GdVO_4$@SiO_2 NPs, and thus, to the FIR calculated from their spectra. Figure 4(b) shows the emission spectra corresponding to the NPs dispersed in water, methanol and DMSO, normalized to the intensity of the $^4S_{3/2} \rightarrow {}^4I_{15/2}$ band. The emission spectrum corresponding to

the dry NPs, measured under the same experimental conditions, is also included for comparison. As can be seen in this graph, the emission intensity of the band located at 520 nm decreases when the NPs are dispersed in a solvent. This might be attributed to more efficient non-radiative relaxation processes in that case that depopulate the $^4S_{3/2}$ level of Er^{3+} towards lower energy emitting levels because of the interactions stablished with the solvation molecules. This also affects to the I_{520} / I_{550} FIR, as can be seen in Figure 4(c), which is reduced by 20 % when compared to that of the powder not dispersed in any solvent. This reduction seems to be similar for NPs dispersed in any of the three solvents analysed in this study, with the smallest values attained in water and DMSO that have a higher dipolar moment.

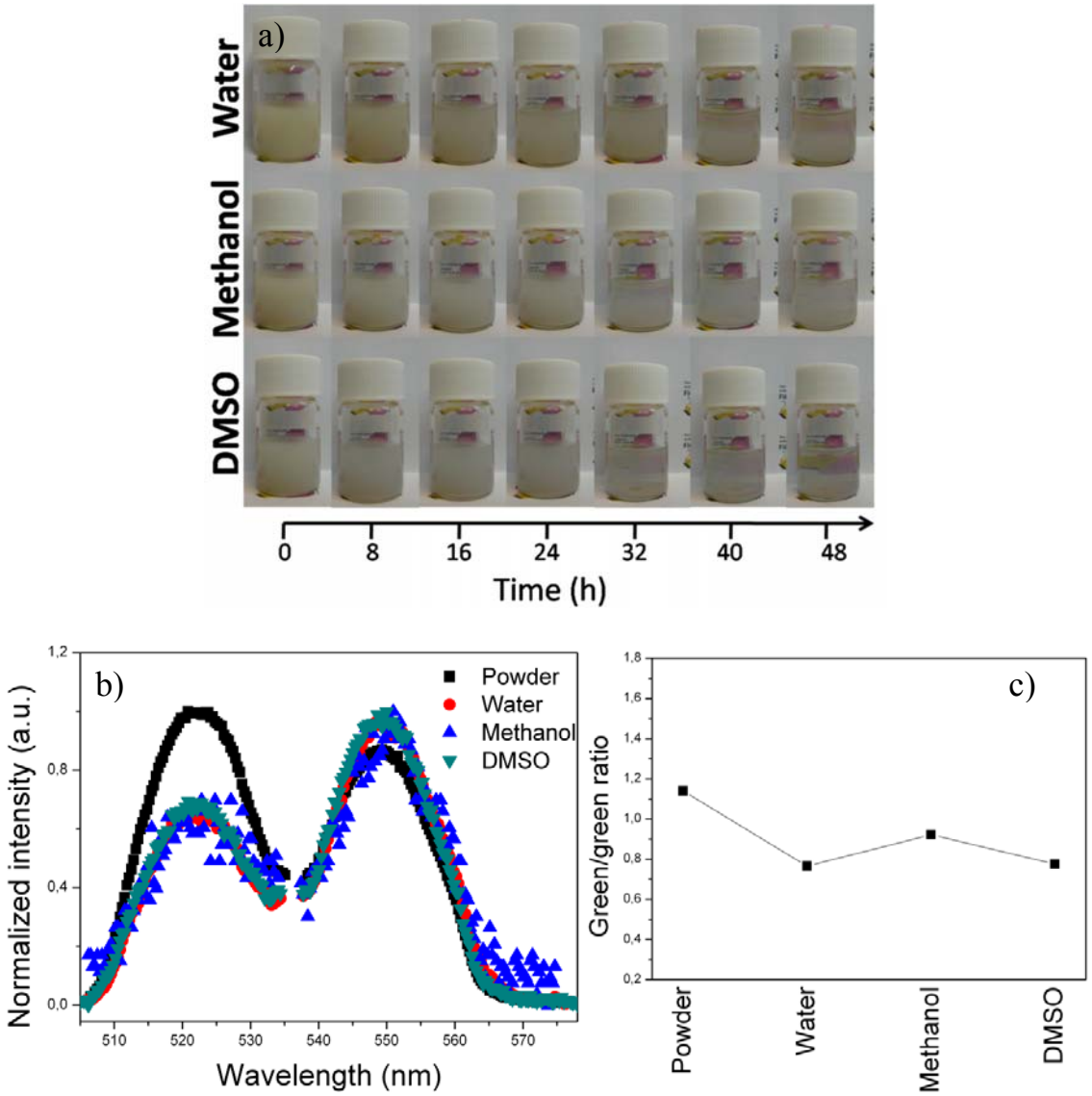

Figure 4.(a) Time evolution of the sedimentation of Er,Yb:$GdVO_4$@SiO_2 nanoparticles dispersed in water, methanol and DMSO; (b) Up-conversion emission spectra of Er,Yb:$GdVO_4$@SiO_2 nanoparticles in different solvents normalized in intensity to the $^4S_{3/2} \rightarrow {}^4I_{15/2}$ band; (c) Green-to-green ($^2H_{4/2} \rightarrow {}^4I_{15/2}$ to $^4S_{3/2} \rightarrow {}^4I_{15/2}$) emission intensity ratios calculated for the core-shell nanoparticles dispersed in the different solvents.

3.5 Ex-vivo experiment to monitor temperature evolution

To probe the potentiality of the use of Er,Yb:$GdVO_4$@SiO_2 core-shell nanoparticles for temperature changes investigation in biological systems, we injected an aqueous dispersion of the nanoparticles (1 wt %) in fresh chicken breast at the depth of around 1-2 mm. A heating gun was used to heat the chicken breast. We monitored the temperature change induced in the chicken breast by observing the luminescence emitted by the injected nanoparticles after excitation with an Apollo Instruments Inc diode laser with emission at 980 nm and a power of 100 mW. The laser was focused on the chicken breast by means of a microscope objective with 40X magnification and N.A. of 0.6. The emission arising from the nanoparticles was collected by the same objective, and after passing a dichroic filter for elimination of the excitation wavelength, was sent to an AVANTES AVS-USB2000 fiberoptic spectrometer connected to a computer to record the spectra. The analysis of the emission spectra and their comparison with the calibration line (see Figure 3b), the temperature was deduced. Moreover, in order to verify the data, the temperature evolution of the chicken breast was also recorded by a digital multimeter connected to the small thermo-resistor Pt-100 located inside the chicken breast, close to the injected nanoparticles. The scheme of the setup is shown in Figure 5a.

The evolution of the temperature with time, during the induced heating process, monitored by using the luminescent nanoparticles and the thermo-resistor Pt-100 are shown in Figure 5b. A fast increase of temperature was clearly observed in both cases. Despite a time delay can be observed in the monitoring process between the thermos-resistor and the luminescent nanoparticles, it is smaller than 1 min, and when the thermal equilibrium is reached, both systems show the same temperature (313 K, with an error of 0.03 K). This experiment

demonstrates the potentiality of using Er,Yb:$GdVO_4$@SiO_2 core-shell nanoparticles for temperature determination purposes in *ex-vivo* biomedical applications with a good thermal resolution.

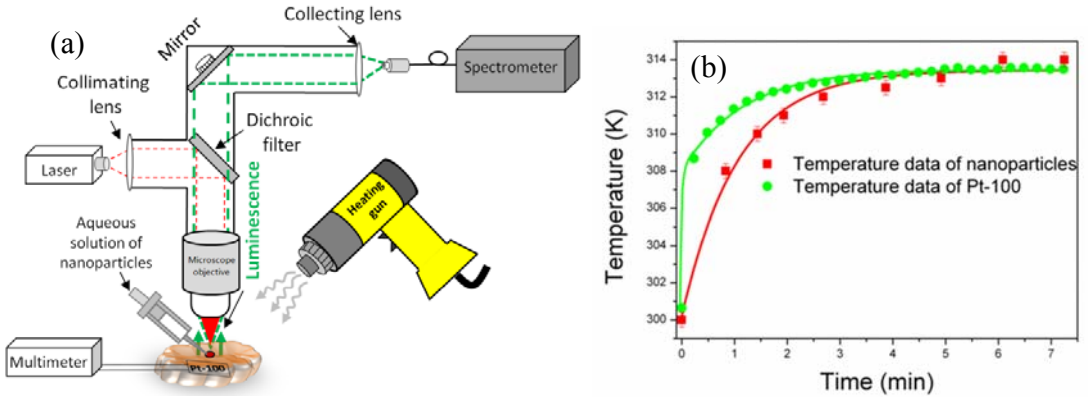

Figure 5. (a) Scheme of the setup for the *ex-vivo* temperature determination experiment; (b) temporal evolution of temperature during the induced heating process in the chicken breast monitored by the Er,Yb:$GdVO_4$@SiO_2 core-shell nanoparticles and a thermo-resistor Pt-100. Lines were plotted to help the reader to follow the temperature evolution.

4. Conclusions

In conclusion, Er,Yb:$GdVO_4$@SiO_2 core-shell NPs can be used as an efficient luminescence temperature sensor. To the best of our knowledge, we have demonstrated for the first time the benefits of a SiO_2 coating on the luminescent thermometric properties. By using a SiO_2 coating, we achieved a ×2 enhancement of the thermal sensitivity. Moreover, the SiO_2 shell protects the NPs from overheating during the excitation process. Also, we demonstrated that a high thermal resolution can be achieved using these core-shell NPs. The spatial resolution is estimated to be of the order of the size of the core-shell NPs. Good stability in different solvents, like water, methanol and DMSO, make possible to use them as a temperature sensor in biological

applications, as the one we reported to monitor an induced heating process in an ex-vivo experiment.

ASSOCIATED CONTENT

SUPPORTING INFORMATION:

Figure S1. X-ray powder diffraction patterns of 1%Tm, 15%Yb:$GdVO_4$ nanoparticles: a) raw sample prepared by 24 h of hydrothermal synthesis at 185 ºC; b) sample after thermal annealing at 873 K during 5 h; c) annealed sample with further coating with a layer of 15-20 nm of silica. For comparison, the X-ray pattern scheme of tetragonal $I4_1/amd$ $GdVO_4$, JCPDS File 86-0996 has been also included in d).

Figure S2. TEM image of hydrothermal Tm, Yb:$GdVO_4$ sample prepared as for the title samples, annealed at 873 K during 5 h and then coated with a thick shell of SiO_2

Figure S3. a) HRTEM image of a polygonal nanoparticle prepared by hydrothermal treatment at 185ºC during 24 h and then annealed at 873 K; b) The corresponding SAED pattern along the [004] zone axis; c) and d) HRTEM images of nanoparticles annealed and coated with a silica shell (light amorphous area around the polygonal nanoparticle).

Figure S4. Comparison of room temperature FT-IR spectra of nanocrystalline tetragonal vanadate samples: a) bare hydrothermal (24h at 185 ºC) prepared sample, b) hydrothermal sample annealed at 873 K during 5 h, c) sample as in b) with further surface coating with a ~7 nm shell of SiO_2.

Figure S5. Distribution by number of the hydrodynamic size of particles in hydrothermal Er, Yb:$GdVO_4$: a) after annealing at 873 K for 5 h, and b) after annealing at 873 K for 5 h and coating with a ~7 nm shell of SiO_2.

Figure S6. Evolution of integrated upconverted luminescence in nanocrystalline 1%Ln, x%Yb:$GdVO_4$ with processing for surface treatments after the hydrothermal synthesis: a) green bands corresponding to $^2H_{11/2}$,$^4S_{3/2}\rightarrow{}^4I_{15/2}$ Er^{3+} transitions, b) blue band corresponding to $^1G_4\rightarrow{}^3H_6$ Tm^{3+} transition. NA = bare non annealed hydrothermal sample, A = annealed at 873 K during 5 h, A+@7 nm SiO_2 = annealed and 7 nm-SiO_2 coated sample, A+@15-20 nm SiO_2 = annealed and 15-20 nm-SiO_2 coated sample.

AUTHOR INFORMATION

Corresponding Author**:** joanjosep.carvajal@urv.cat

Authors Contributions

The manuscript was written through contributions of all authors. All authors have given approval to the final version of the manuscript

Notes

The authors declare no competing financial interests.

ACKNOWLEDGMENTS

This work was supported by the Spanish Government under Projects No. MAT2013-47395-C4-4-R, TEC2014-55948-R and MAT2014-56607-R, and by Catalan Authority under Project No. 2014SGR1358. Ol. A. Savchuk is supported by Catalan Government through the fellowship 2015FI B2 00136. F.D. acknowledges additional support through the ICREA Academia award 2010ICREA-02 for excellence in research.

REFERENCES

(1) Hildebrandt, B.; Wust, P.; Ahlers, O.; Dieing, A.; Sreenivasa, G.; Kerner, T.; Felix R.; and Riess, H. The Cellular and Molecular Basis of Hyperthermia. *Crit. Rev. Oncol. Hematol.* **2002**, *43*, 33–56.

(2) Roti Roti, J. L. Cellular Responses to Hyperthermia (40-46 degrees C): Cell Killing and Molecular Events. *Int. J. Hyperthermia* **2008**, *24*, 3–15.

(3) Brites, C. D. S.; Lima, P. P.; Silva, N. J. O.; Millan, A.; Amaral, V. S; Palacio, F.; and Carlos, L. D. Thermometry at the Nanoscale. *Nanoscale* **2012**, *4*, 4799-4829.

(4) Jaque, D.; Vetrone, F. Luminescence Nanothermometry. *Nanoscale* **2012**, *4*, 4301–4326.

(5) Wade, S. A.; Collins, S. F.; Baxter, G. W. The Fluorescence Intensity Ratio Technique for Optical Fiber Point Temperature Sensing. *J. Appl. Phys.* **2003**, *94*, 4743-4756.

(6) Vetrone, F.; Naccache, R.; Zamarron, A.; de la Fuente, A. J.; Sanz-Rodriguez, F.; Maestro, L. M.; Rodriguez, E. M.; Jaque, D.; Sole, J. G.; Capobianco, J. A. Temperature Sensing at the Nanoscale using Fluorescent Nanothermometers. *ACS Nano* **2010**, *4*, 3254–3258.

(7) Vetrone, F.; Naccache, R.; de la Fuente, A. J.; Sanz-Rodrıguez, F.; Blazquez-Castro, A.; Rodriguez, E. M.; Jaque, D.; Sole, J. G.; Capobianco, J. A. Intracellular Imaging of HeLa Cells by Non-Functionalized $NaYF_4$:Er^{3+},Yb^{3+} Upconverting Nanoparticles. *Nanoscale* **2010**, *2*, 495–498.

(8) Haro-Gonzalez, P.; Maestro, L. M.; Trevisani, M.; Polizzi, S.; Jaque, D.; Sole, J. G.; Bettinelli, M. Evolution of Rare Earth Doped Silica Sub-Micrometric Spheres as Optically Controlled Temperature Sensors. *J. Appl. Phys.* **2012**, *112*, 054702-054709.

(9) Wang, X.; Kong, X. G.; Yu, Y.; Sun, Y. J.; Zhang, H. Effect of Annealing on Upconversion Luminescence of ZnO:Er^{3+} Nanocrystals and High Thermal Sensitivity. *J. Phys. Chem. C* **2007**, *111*, 15119−15124.

(10) Alencar, M. A. R.; Maciel, G. S.; de Araújo, C. B.; Patra, A. Er^{3+}-Doped $BaTiO_3$Nanocrystals for Thermometry: Influence of Nanoenviroment on the Sensitivity of a Fluorescence Based Temperature Sensor. *Appl. Phys. Lett.* **2004**, *84*, 4753−4755.

(11) dos Santos, P. V.; de Araujo, M. T.; Gouveia-Neto, A. S.; Neto, J. A. M.; Sombra, S. B. Optical Thermometry Through InfraredExcited Upconversion Fluorescence Emission in

Er^{3+} and Er^{3+}-Yb^{3+}-doped Chalcogenide Glasses. *IEEE J. Quantum Electron.* **1999**, *35*, 395−399.

(12) Debasu, M. L.; Ananias, D.; Pastoriza-Santos, I.; Liz-Marzán, L. M.; Rocha, J.; Carlos, L. D. All-in-One Optical Heater-Thermometr Nanoplatform Operative From 300 to 2000 K Based in Er^{3+} Emission and Blackbody Radiation. *Adv. Mater.* **2013**, *25*, 4868−4874.

(13) Aigouy, L.; Saidi, E.; Lalouat, L.; Labeguerie-Egea, J.; Mortier,M.; Low, P.; Bergaud, C. AC Thermal Imaging of a Microwire with a Fluorescent Nanocrystal: Influence of the Near Field on the Thermal Contrast. *J. Appl. Phys.* **2009**, *106*, 074301-074310.

(14) Saïdi, E.; Samson, B.; Aigouy, L.; Volz, S.; Low, P.; Bergaud, C.; Mortier, M. Scanning Thermal Imaging by Near-Field Fluorescence Spectroscopy. *Nanotechnology* **2009**, *20*, 115703.

(15) Li, C. R.; Dong, B.; Ming, C. G.; Lei, M. Application to Temperature Sensor Based on Green Up-Conversion of Er^{3+} Doped Silicate Glass. *Sensors* **2007**, *7*, 2652−2659.

(16) Maciel, G. S.; Menezes, L. d. S.; Gomes, A. S. L.; de Araujo, C.B.; Messaddeq, Y.; Florez, A.; Aegerter, M. A. Temperature Sensor Based on Frequency Upconversion in Er^{3+}-Doped Fluoroindate Glass. *IEEE Photonics Technol. Lett.* **1995**, *7*, 1474−1476.

(17) Singh, S. K.; Kumar, K.; Rai, S. B. Er^{3+}/Yb^{3+}Codoped Gd_2O_3Nano-Phosphor for Optical Thermometry. *Sens. Actuators A* **2009**, *149*, 16−20.

(18) Li, C. R.; Dong, B.; Li, S. F.; Song, C. Er^{3+}-Yb^{3+} Co-Doped Silicate Glass for Optical Temperature Sensor. *Chem. Phys. Lett.* **2007**,*443*, 426−429.

(19) Fischer, L. H.; Harms, G. S.; Wolfbeis, O. S. Upconverting Nanoparticles for Nanoscale Thermometry. *Angew. Chem. Int. Ed.* **2011**, *50*, 4546-4551.

(20) Huang, J.; He, B.; Cheng, Z.; Zhou, L. *J. Lumin.* **2015**, *160*, 254-257.

(21) Brites, C. D. S.; Lima, P. P.; Carlos, L. D. *J. Lumin* **2015** http://dx.doi.org/10.1016/j.jlumin.2015.01.025.

(22) Prorok, K.; Bednarkiewicz, A.; Cichy, B.; Gnach, A.; Misiak, M.; Sobczyk, M.; Strek, W.; The Impact of Shell Host ($NaYF_4/CaF_2$) and Shell Deposition Methods on the Up-Conversion Enhancement in Tb^{3+}, Yb^{3+}Codoped Colloidal α-$NaYF_4$ Core-Shell Nanoparticles. *Nanoscale* **2014**, *6*, 1855-1864.

(23) Bertini, C.; Toncelli, A.; Tonelli, M.; Cavalla, E.; and Magnani, N. *J. Lumin.* **2004**, *106*, 235-242.

(24) Calderon-Villajos, R.; Zaldo, C.; and Cascales, C. Enhanced Upconversion Multicolor and White Light Luminescence in SiO_2-Coated Lanthanide-Doped $GdVO_4$ Hydrothermal Nanocrystals. *Nanotechnology* **2012,** *23,* 505205-505215.

(25) Dong, N. N.; Pedroni, M.; Piccinelli, F.; Conti, G.; Sbarbati, A.; Ramírez-Hernández, J. E.; Martínez Maestro, L.; Iglesias-de la Cruz, M.C.; Sanz-Rodriguez, F.; Juarranz, A.; Chen, F.; Vetrone, F.; Capobianco, J. A.; García Solé, J.; Bettinelli, M.; Jaque, D.; and Speghini, A. *ACS Nano* **2011**, *5*, 8665-8671.

(26) Dong, B.; Cao, B.; He, Y.; Liu, Z.; Li, Z.; Feng, Z. Temperature Sensing and In Vivo Imaging by Molybdenum Sensitized Visible Upconversion Luminescence of Rare-Earth Oxides. *Adv. Mater.* **2012**, *24* 1987-1993.

(27) Sedlmeier, A.; Achatz, D.E.; Fischer, L.H.; Gorris, H.H.; Wolfbeis, O.S. *Nanoscale* **2012**, *4*, 7090-7096.

(28) Wang, Z.; Ananias, D.; Carne-Sanchez, A.; Brites, C. D. S.; Imaz, I.; Maspoch, D.; Rocha, J.; and Carlos, L. D. *Adv. Func. Mater.* **2015**, *25* 2824-2830.